

## Two-Dimensional Real-Space Analysis of Optical Excitations in Acceptor-substituted Carotenoids.

Sergei Tretiak, Vladimir Chernyak, and Shaul Mukamel\*

*Contribution from the Department of Chemistry, and Rochester Theory Center for Optical Science and Engineering, University of Rochester, Rochester, New York 14627*

*Received June 18, 1997, Revised Manuscript Received August 21, 1997* <sup>⊗</sup>

**Abstract:** Absorption spectra of substituted carotenoids with varying acceptor strength are analyzed using collective electronic normal modes obtained using the time-dependent Hartree-Fock (TDHF) technique combined with the INDO/S semiempirical hamiltonian. Two-dimensional plots of the collective excitations in real space show an *off-diagonal size* associated with relative motion of electron-hole pairs created upon optical excitation and a *diagonal size* representing the pair's center of mass motion. By varying the polyene chain length we show that the response of symmetric molecules is controlled by "bulk" delocalized excitations with coherence size  $\sim 12$  double bonds whereas the response of short polar molecules is dominated by a localized "charge-transfer" excitation created at the acceptor end with coherence and diagonal lengths  $\sim 12$  and  $\sim 17$  double bonds respectively.

### I. INTRODUCTION

Substituted conjugated molecules have interesting optical properties which reflect the interplay of the donor-acceptor strength and the type and length of the connecting bridge [1-5]. The charge-transfer, energy-transfer, and isomerization of such systems have been thoroughly investigated and form the basis for our understanding of the photophysics and photochemistry of complex molecules [6-8]. Many photophysical and photochemical biological processes involve conjugated chromophores such as porphyrins and chlorophylls. The nonlinear optical properties of these systems have also been studied in search for new organic optical materials with large nonlinear polarizabilities [4,5,9-14].

In this article we calculate and analyze the electronic spectra of a family of acceptor substituted carotenoids [11] using the recently developed collective electronic oscillator (CEO) approach [15-18]. The carotenoids form one of the most important groups of natural pigments, and are found in all families of vegetables and animal kingdoms [19,20]. In photosynthetic cells these molecules appear in antenna complexes that absorb the light and transfer excitation to the reaction centers [21,22]. In ad-

dition they serve as antioxidants by quenching the chlorophyll triplet via energy transfer and preventing the formation of singlet oxygen. The photoisomerization of the closely related retinoids plays a role in various physiological functions (e.g. the primary process of vision) [21,23].

The theoretical interpretation of spectroscopic measurements usually involves an extensive numerical effort. The optical response of organic molecules is traditionally represented in terms of their global many-electron eigenstates [24,25]. The techniques used to calculate these eigenstates are usually limited by computational time and memory to small molecules. For example, the Configuration-Interaction / Sum-over-States (CI/SOS) method [1,10] based on the expansion of the Stark energy of the molecule in powers of electric field, involves the calculations of both the ground state and excited states wavefunctions and the transition dipole moments between them. The global eigenstates carry too much information about the system, which makes it hard to use them efficiently in the interpretation of optical response and in the prediction of various trends. Many of the interesting ground state properties may be explained by the reduced single-electron density matrix [26,27]

$$\bar{\rho}_{mn} \equiv \langle g | c_m^+ c_n | g \rangle, \quad (1.1)$$

where  $c_m^+$  ( $c_m$ ) are creation (annihilation) operators of an electron at the  $m$ 'th atomic orbital, and  $|g\rangle$  is the ground state many-electron wavefunction. The diagonal elements  $\bar{\rho}_{nn}$  represent the electronic charge density at the  $n$ 'th orbital. These elements are used in various population analyses (Löwdin, Milliken) to prescribe a portion of charge to specific atoms and are commonly visualized using contour charge density maps. The off-diagonal elements,  $m \neq n$ , represent the bonding structure (i.e. bond orders) associated with a pair of atomic orbitals and are useful in interpreting the chemical bonding pattern along the molecule [28-31]. In the CEO approach presented here, the microscopic electronic dynamics underlying the optical transitions between the ground state and an electronic excited state  $|\nu\rangle$  is expressed using the matrix  $\xi_\nu$ , with matrix elements

$$(\xi_\nu)_{mn} = \langle \nu | c_m^+ c_n | g \rangle. \quad (1.2)$$

The optical response involves only reduced information about the global eigenstates. This information is contained in the matrices  $\xi_\nu$ . To see this we note that the

<sup>⊗</sup> Abstract published in *Advance ACS Abstracts*, November 1, 1997

molecular dipole is a single-electron operator which may be expanded in the form

$$P = \sum_{mn} \mu_{mn} c_m^+ c_n, \quad (1.3)$$

where  $\mu_{mn}$  is the transition dipole matrix element. The frequency-dependent linear polarizability  $\alpha(\omega)$  then assumes the form

$$\alpha(\omega) = \sum_{\nu} \sum_{mnkl} \mu_{mn} \mu_{kl} \frac{2\Omega_{\nu}(\xi_{\nu})_{mn}(\xi_{\nu})_{kl}}{\Omega_{\nu}^2 - (\omega + i\Gamma)^2} \quad (1.4)$$

where  $\Gamma$  is a relaxation rate and  $\nu$  label global excited eigenstates  $|\nu\rangle$  with energies  $E_{\nu}$  and transition frequencies  $\Omega_{\nu} \equiv E_{\nu} - E_g$ . Eq.(1.4) implies that the matrices  $\xi_{\nu}$  and the corresponding frequencies  $\Omega_{\nu}$  contain all necessary information for calculating the linear optical response. Calculating  $\xi_{\nu}$  through Eq. (1.2) implies that we first need to calculate the eigenstates  $|\nu\rangle$  and  $|g\rangle$  and then use them to compute the matrix element. However, we will calculate the matrices  $\xi_{\nu}$  and frequencies  $\Omega_{\nu}$  directly using the time-dependent Hartree-Fock (TDHF) approach which allows us to avoid the tedious calculations of global eigenstates [15,18,17]. The TDHF scheme is based on calculating the time-dependent density matrix

$$\begin{aligned} \rho_{mn}(t) &\equiv \langle \Psi(t) | c_m^+ c_n | \Psi(t) \rangle \\ &= \bar{\rho}_{mn} + \sum_{\nu} a_{\nu}(t)(\xi_{\nu})_{mn} + a_{\nu}^*(t)(\xi_{\nu}^+)_{mn}, \end{aligned} \quad (1.5)$$

where  $\Psi(t)$  is the many-electron wave-function of the molecule driven by the external field. The matrices  $\xi_{\nu}$  appear as eigenmodes of the linearized TDHF equation with frequencies  $\Omega_{\nu}$ . The diagonal elements of  $\xi_{\nu}$  ( $n = m$ ) represent the net charge induced on the  $n$ 'th atomic orbital by an external field, whereas  $(\xi_{\nu})_{mn}$   $n \neq m$  is the dynamical bond-order representing the joint amplitude of finding an electron on orbital  $m$  and a hole on orbital  $n$ . We shall refer to  $\xi_{\nu}$  as *electronic normal mode* since they represent collective motions of electrons and holes. They are the electronic analogues of vibrational normal modes used in the interpretation of infrared and Raman spectra. By displaying the matrices  $\xi_{\nu}$  using two-dimensional plots we establish a direct real-space connection between the optical response and motions of charges in the molecule upon optical excitation. The electronic modes carry less information than the global eigenstates but substantially more than required for calculating molecular polarizabilities. The matrix elements  $\mu_{mn}$  of the polarization operator are nonzero only for overlapping orbitals, which is the case when orbitals  $m$  and  $n$  are centered either on the same atom or on nearest neighbors in the molecular structure. Eqs.(1.4) and (1.2) then imply that  $\alpha(\omega)$  only requires near-diagonal matrix elements of  $\xi_{\nu}$ . However in order to develop a clear physical picture of the optical response it is essential to consider all matrix elements of the modes (including those that do

not contribute directly to  $\alpha(\omega)$  since  $\mu_{mn} = 0$ ). Another notable advantage of the CEO approach is that, unlike CI calculations, it is size-consistent. This implies that all calculated properties will show the proper scaling with size in the large molecule limit.

Our analysis shows that it is very difficult to disentangle the effects of donor-acceptor and bridge length on the spectroscopy of molecules with relatively short bridges. To obtain a clear picture of the optical response of acceptor-substituted molecules we found it instructive to study the size-dependence of optical properties starting with very long bridges. In these systems the effects of the acceptor and the bridge regions can be clearly separated. Optical properties of acceptor-substituted molecules with shorter bridges can then be attributed to quantum confinement, which is important when the bridge size becomes comparable to the coherence length  $L_I$ . This analysis is reminiscent of the description of exciton confinement in semiconductor nanostructures [32] where  $L_I$  is given by the Wannier exciton diameter [33–35].

In Section II we investigate the ground-state properties of several acceptor - substituted carotenoids studied experimentally in [36,11], using the ground-state density matrix calculated from the INDO/S hamiltonian, as described in Appendix A. Real-space analysis of the optical response of these molecules is carried out in Section III by solving the TDHF equations which use the ground state density matrices and as an input. Details of the calculations are given in Appendices B – D. Previous applications of the CEO were based on the Pariser-Par-Pople (PPP) hamiltonian which is parameterized to a limited class of molecules. The combination with the INDO/S hamiltonian presented here allows us to calculate the optical properties of a broad range of molecules without tuning any empirical parameters. Linear absorption and off-resonant quadratic and cubic polarizabilities of these molecules are calculated, and their scaling with size in neutral and polar molecules are investigated using two-dimensional plots of the dominant electronic modes. In Section IV the ground-state properties of large donor-acceptor substituted molecules are analyzed. Finally we discuss and summarize our results in Section V.

## II. SIZE-SCALING OF THE GROUND -STATE DENSITY MATRIX.

The six carotenoids listed in order of increasing acceptor-strength in Fig. 1 were synthesized and their optical electronic spectra measured in [36]. Betacarotene (1) is a symmetric nonpolar molecule. In the other molecules one end was substituted with an acceptor group.

We first calculated the Hartree-Fock ground-state density matrices. Optimal ground-state geometries were obtained at the AM1 level using Gaussian-94. The ZINDO

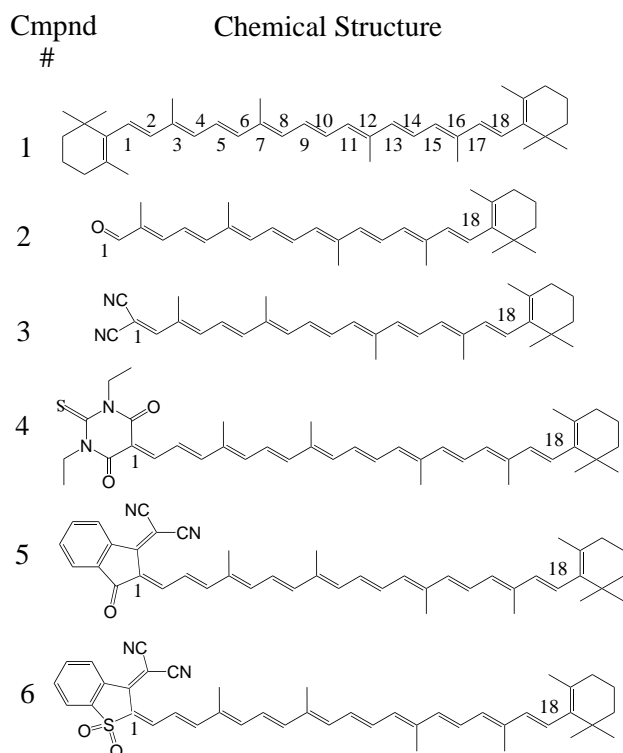


FIG. 1. Six acceptor-substituted carotenoids [11,36] listed in order increasing acceptor strength. Repeat units numbering used in two-dimensional plots is given for molecule 1.

code was used next to generate the INDO/S hamiltonian (Appendix A). This Hamiltonian assigns a single  $s$ -type basis function to hydrogen atoms and four basis functions ( $s, p_x, p_y, p_z$ ) to all other heavy atoms of these molecules. The orbitals  $s, p_y, p_z$  on the carbons in the chain are  $sp^2$  hybridized and form the molecular  $\sigma$ -bonding skeleton. Qualitatively, only  $p_x$  orbitals perpendicular to the molecular plane participate in the  $\pi$ -bonding network and are responsible for the lowest optical excitations. Assuming that  $\sigma$ -electrons do not contribute to the ground state acceptor - bridge charge redistribution and to the optical properties, we sorted out all  $K \times K$  ( $K$  being the total basis set size) density matrices, retaining only elements corresponding to  $p_x$  orbitals. The resulting  $k \times k$  matrices (where  $k < K$  is the number of  $p_x$  orbitals of heavy atoms) were displayed as contour plots. The ground state density matrix elements have the following physical significance: the diagonal elements ( $n = m$ ) represent the  $\pi$ -electron charge at the  $m$ 'th atom, whereas the off-diagonal ( $n \neq m$ ) elements reflect the  $\pi$ -bond-orders between  $n$  and  $m$  atoms<sup>1</sup>. We

<sup>1</sup>This applies for the polyenic chain but not to some atoms at the ends of molecules, where other types of hybridizations are formed. Since our goal is to explore the dynamics of the  $\pi$ -electron system in the chain, we will use this interpretation.

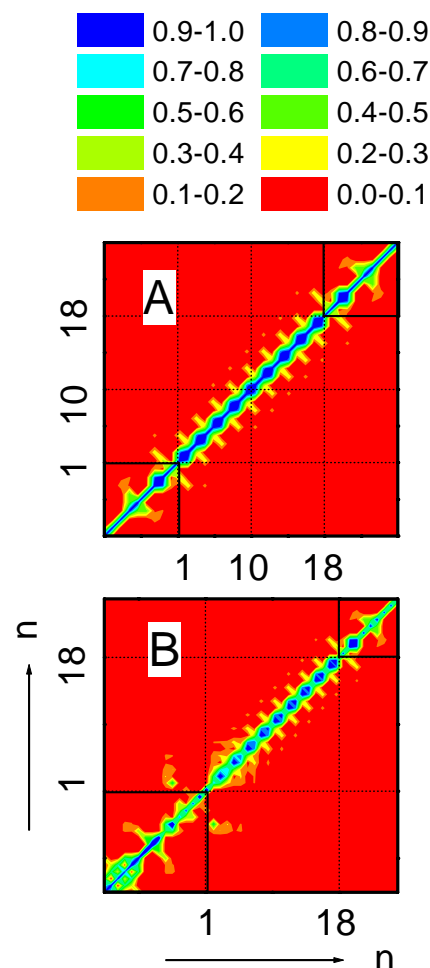


FIG. 2. Contour plots of ground state density matrices for (A) neutral  $N(10)$  (compound 1) and (B) polar  $P(10)$  (compound 6) molecules. The color code is shown in the upper panel. The structures at the ends of molecules are shown by rectangles.

thus end up with the same interpretation of the density matrices as used previously for the simpler PPP hamiltonian [37,17].

The effect of the acceptor on the molecular ground state can be interpreted by using contour plots of the density matrices. The absolute values of the reduced single-electron ground-state density matrix elements  $|\bar{\rho}_{nm}|$  of beta-carotene (1) are shown in Fig. 2A. The axes represent carbon atoms. (The bridge atoms are labeled 1-18 as indicated in Fig. 2). The parts corresponding to the end structures are marked by rectangles in the corners of matrix. The chain's density matrix is dominated by the diagonal and near-diagonal elements, reflecting the bonds between nearest neighbors. The nine bridge double bonds and two double bonds located at the ends are clearly identified. The ground-state density matrix of molecule 6 (with the strongest acceptor) is displayed in Fig. 2B. The decrease of  $\pi$ -electron density in the bridge (along the diagonal of the matrix) near the acceptor is

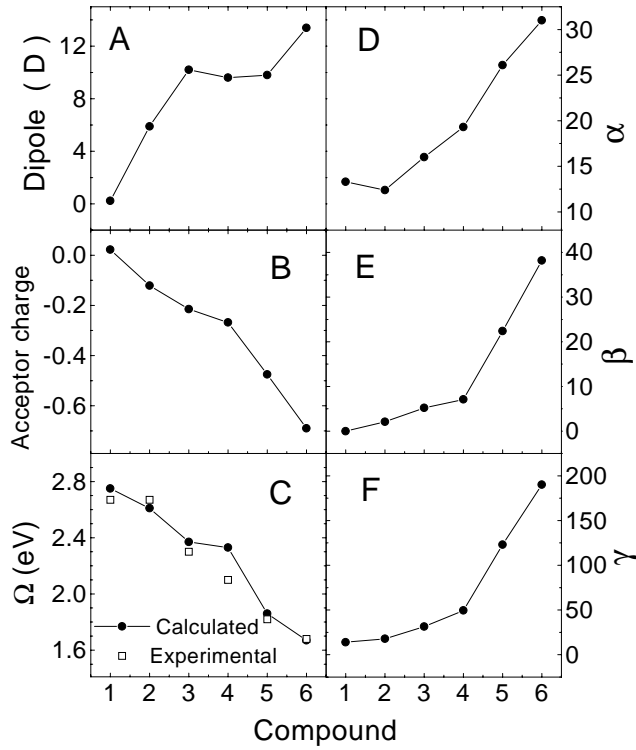


FIG. 3. Dipole moments (A), total charge on the acceptor (B), frequency of the lowest transition (C), linear  $\alpha(0)$  (D), quadratic  $\beta(0)$  (E), and cubic  $\gamma$  (F) off-resonant polarizabilities for six carotenoids. The ordinate axes are labeled by compound number according to Fig.1.  $\alpha$ ,  $\beta$ , and  $\gamma$  are in the units of  $e\text{\AA}^2V^{-1}$  [ $1.441 \times 10^{-23} \text{ esu}$ ],  $e\text{\AA}^3V^{-2}$  [ $4.323 \times 10^{-29} \text{ esu}$ ], and  $e\text{\AA}^4V^{-3}$  [ $1.297 \times 10^{-34} \text{ esu}$ ] respectively.

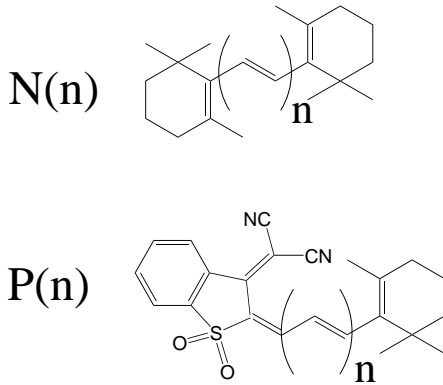


FIG. 4. Structures of the neutral  $N(n)$  and polar  $P(n)$  (substituted by the strongest acceptor) molecules. Calculations were done for chain lengths of  $n = 10, 15, 20, 30, 40$  double bonds.

clearly seen. Other calculated ground-state properties of all molecules are displayed in Fig. 3. The growth of ground-state dipole moments (panels A) and the total charge on the acceptor end (panels B) is commensurate with increasing the acceptor strength.

To explore the acceptor effect we examined the size-

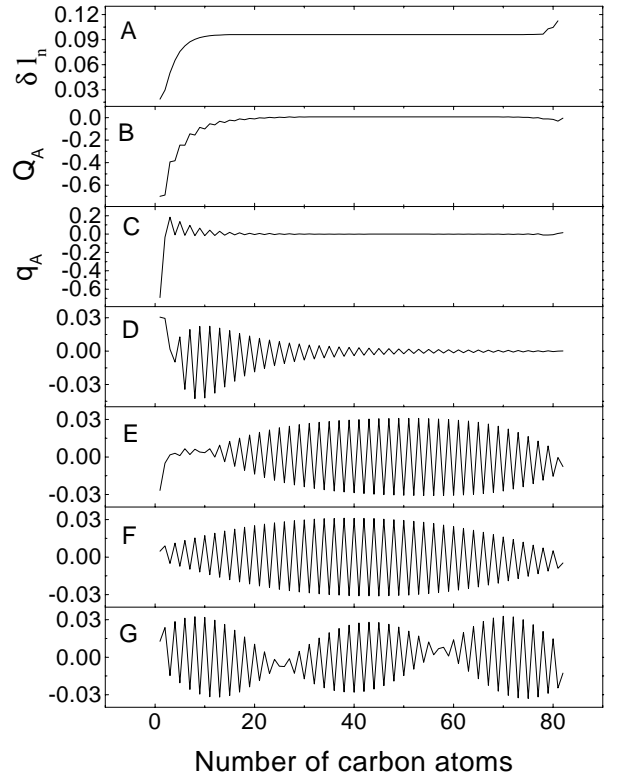


FIG. 5. Variation of the bond-length alternation (A), total charge  $Q_A$  (B), total atomic charge  $q_A$  (C), diagonal elements of modes  $a$  and  $b$  in polar  $P(n)$  molecule (D and E), and modes  $a'$  and  $b'$  in neutral  $N(n)$  molecule (F and G)) along the chain for chain length  $n = 40$  double bonds.

scaling of the optical response and its saturation to the bulk by increasing the polyenic chain length.<sup>2</sup> The molecular templates shown in Fig. 4 represent two extreme cases: neutral  $N(n)$  and polar  $P(n)$  molecules. Some ground state properties of  $P(40)$  are displayed in Fig. 5. We first consider the bond-length alternation parameter  $\delta l_j$  which denotes the difference between the single ( $l_{2j}$ ) and the double ( $l_{2j-1}$ ) bond lengths in the  $j$ 'th repeat unit along the bridge

$$\delta l_j = l_{2j} - l_{2j-1}, \quad j = 1, \dots, n. \quad (2.1)$$

(Note that the first repeat unit  $j = 1$  is at the acceptor end.) Panel A shows the variation of the bond-length alternation along the bridge. Panel C represents the variation of the total atomic charge  $q_A$  (Eq. (B1)) along the chain, and panel B shows the integral of this quantity

$$Q_A = Q_{\text{Acceptor}} + \sum_{a=1}^A q_a, \quad (2.2)$$

<sup>2</sup>During geometry optimization in long molecules, the geometry of the polyenic chain was constrained to be planar.

where  $Q_{\text{Acceptor}} = 0.69e$  is the total electronic charge on the acceptor. These calculations illustrate the interplay of bulk and boundary (end) effects in electronic structure of conjugated molecules. The figures show that the acceptor attracts electronic charge and attempts to invert the chain structure to zwitterionic. The  $\pi$ -electronic system in response screens the acceptor influence by inducing a positive charge at the acceptor end. The electrons completely neutralize the acceptor at an effective length of about 10 double bonds, and the other parts of the molecule are unaffected by the acceptor. This leads to a saturation of the ground - state dipole moment at this molecular size.

The acceptor-strength controls the magnitude of the dipole moment whereas the electronic mobility determines the effective screening length. Our analysis is based on following the charge distribution  $q_A$  and bond-length alternation  $\delta l_n$  along the chain. The bond-order alternation, which is another important characteristic of electronic structure, is usually strongly correlated with the bond-length alternation  $\delta l_n$  [38], and for the sake of brevity we have used  $\delta l_n$  as the measure of both quantities. In the next section we will use the ground-state density matrices to calculate and interpret the optical spectra of these molecules.

### III. ELECTRONIC NORMAL MODES AND OPTICAL ABSORPTION

The experimental absorption spectra of the family of substituted carotenoids (Fig. 1) are displayed in Fig. 6 (dashed lines) [36]. The spectrum of the unsubstituted molecule (1) is dominated by a single peak *a*. As the acceptor strength is increased, this peak is red shifted and a second, weaker, peak *b* appears. An additional impurity peak *i*, appearing around 4.5 eV on all experimental spectra (and absent in our calculations), originates from the anti-oxidant added to samples in order to increase their shelf lifetime. Nonlinear polarizabilities of these molecules showed a dramatic growth with increasing acceptor strength.

The absorption spectra were calculated by solving the TDHF equations outlined in Appendix B, using the ground-state density matrices  $\bar{\rho}$  as an input. The electronic modes  $\xi_\nu$  (Appendix C) were calculated using the DSMA outlined in Appendix D. We have recasted Eq. (1.4) in the form

$$\alpha(\omega) = \sum_{\nu} \frac{f_{\nu}}{\Omega_{\nu}^2 - (\omega + i\Gamma)^2}, \quad (3.1)$$

where  $f_{\nu} = 2\Omega_{\nu} \text{Tr}(\mu\xi_{\nu})^2$  is the oscillator-strength of the  $g$  to  $\nu$  transition. The six calculated spectra shown by solid lines in Fig. 6 closely resemble the experimental spectra. The red-shift of the band edge transition (*a*) with increasing acceptor strength is completely reproduced: computed frequencies are within 0.07 eV of ex-

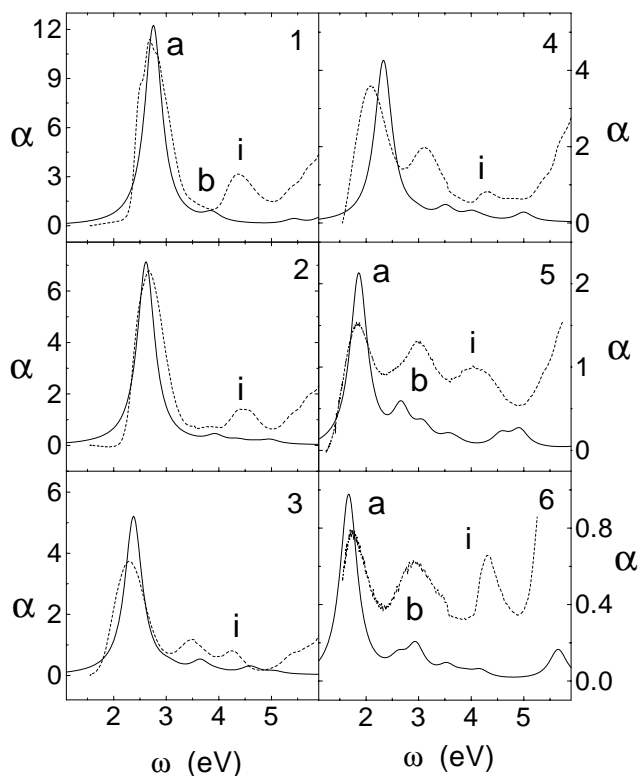


FIG. 6. Calculated (solid lines) and experimental (dashed lines) linear absorption spectra [36] of six carotenoids. Panels are numbered according to Fig.1. The absolute values of linear polarizability are given in arbitrary units. Theoretical spectra were calculated with linewidth  $\Gamma = 0.2$  eV. Peak *i* at 4.5 eV appearing on all experimental spectra originates from the anti-oxidant added to samples

periment, except for compound 4 where the difference is 0.23 eV (see panel C in Fig. 3). The second peak (*b*) was reproduced in our calculations with a weaker oscillator strength compared with experiment. This discrepancy may be attributed to two factors: First, as will be shown later, an acceptor perturbs the second charge - transfer mode which is dark in the symmetric molecule, and makes it visible in linear absorption. This influence depends not only on the acceptor strength, but also on  $\pi$ -electron mobility, which in turn depends on the bond - length alternation (in non-alternating chains the electrons move more easily). Calculations performed with slightly different geometries (obtained from different levels of semiempirical or *ab initio* geometry optimizations) showed that the relative oscillator-strengths of these peaks in molecules with strong acceptors are much more sensitive to the bond - length alternation than their frequencies (the second peak (*b*) became comparable and even stronger than the first peak (*a*) for some geometries). Therefore, even small differences between experimental and calculated structures can lead to the redistribution of intensity of the linear absorption peaks. Second, the experiments, were carried out in films where intermolecular interactions, which were not taken into ac-

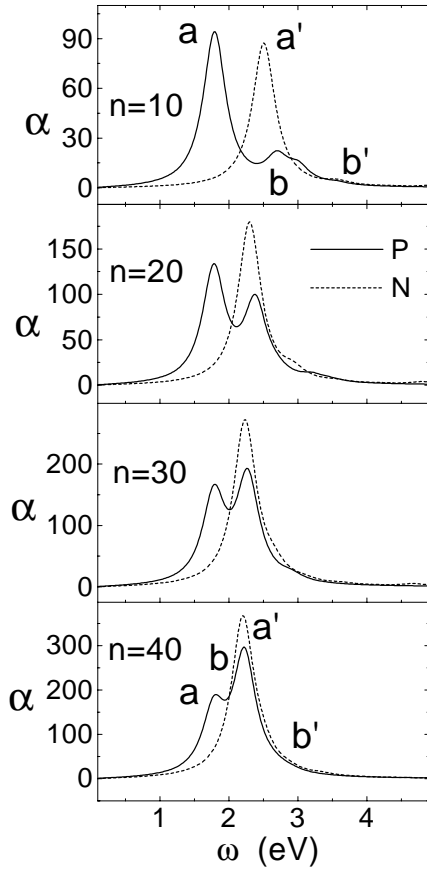


FIG. 7. Linear absorption spectra calculated with linewidth  $\Gamma = 0.2$  eV of the neutral  $N(n)$  (dashed lines) and polar  $P(n)$  (solid lines) molecules shown in Fig. 4. The relative values of linear polarizability are given in arbitrary units.

count in the present single-molecule calculations, may be significant. For example, intermolecular charge transfer [39] is possible between the acceptor and the neutral end of an adjacent molecule.

The right column in Fig. 3 shows the variation of the off-resonant first, second, and third order polarizabilities  $\alpha(0)$ ,  $\beta(0)$ , and  $\gamma(0)$  with acceptor strength. We found a steep growth  $\alpha(0)$  and  $\gamma(0)$  by factors 2.5 and 15 respectively from neutral to the most polar case. Experimentally the compound with the strongest acceptor showed a 45-fold enhancement of resonant  $\gamma$  compare to the neutral betacarotene [11]. To explore this strong acceptor effect on the polarizabilities we examined the size-scaling and saturation to the bulk of the optical response in molecules  $P(n)$  and  $N(n)$ . We expect the acceptor's influence to decrease with increasing molecular size, and in the infinite chain limit all molecules should have the same linear absorption spectra with the saturated band-edge transition  $\Omega_\infty$  and bulk scaling of linear polarizability  $\alpha \sim n$  [38,40]. Starting with  $N(40)$  and  $P(40)$ , we gradually decreased the chain length and followed the evolution of the optical response up to 10 double bonds which is the bridge length of carotenes 1 and 6. The electronic absorption of

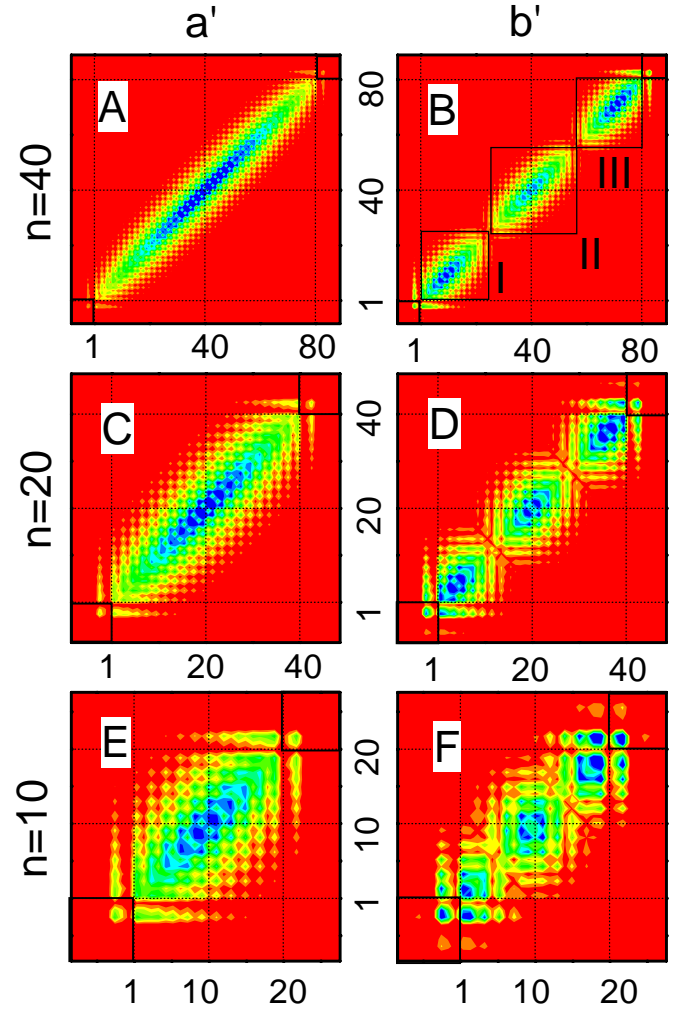


FIG. 8. Contour plots of density matrices for neutral  $N(n)$  molecule. Top panel: coordinates of the first  $a'$  (A) and second  $b'$  (B) absorption peaks for chain length  $n = 40$  double bonds. Middle and bottom panels display the same quantities but for chain lengths of  $n = 20$  and  $n = 10$  double bonds, respectively. The structures at the ends of molecules are shown by rectangles.

$P(n)$  (solid lines) and  $N(n)$  (dashed lines) are displays in Fig. 7 for  $n=40,30,20$ , and 10 double bonds. The figure clearly shows that the oscillator - strength of the lowest frequency peak  $a$  of the polar molecules does not change considerably whereas the second peak  $b$  grows with increasing chain length and gradually attains the bulk limit of the band edge  $a'$  transition of the neutral molecules.

To account for these trends we display in Figures 8 and 10 the absolute magnitudes of the electronic modes  $\xi_\nu$  corresponding to both peaks using the same format of the ground state calculations (Fig. 2). These two-dimensional plots allow us to gain a clear physical insight into the nature of optical excitations. By displaying the matrices representing the modes in the site representation we relate the optical properties directly to motions of charges in the system. Optical excitations create

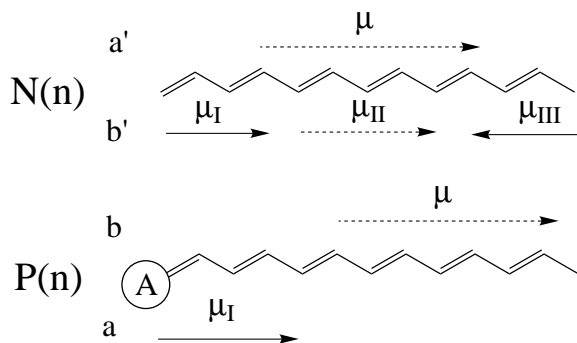


FIG. 9. Sketch of the dipole moments  $\mu = Tr(\mu Q)$  gain for dominant modes in neutral  $N(n)$  and polar  $P(n)$  molecules with chain length  $n = 40$  double bonds.

electron-hole pairs; The ordinate and abscissa label electron and hole respectively. The diagonal elements  $\xi_{mn}$  reflect induced charges on various atoms whereas the off-diagonal elements  $\xi_{mn}$  show the probability amplitude of finding an excess electron at the  $m$ -th atomic orbital and a hole on the  $n$ -th atomic orbital.

The electronic modes of the two strongest transitions  $\xi_{a'}$  and  $\xi_{b'}$  appearing in the spectra of neutral molecules  $N(40)$  (panels A and B)  $N(20)$  (panels C and D) and  $N(10)$  (panels E and F) are displayed in Fig. 8. The electronic modes of the neutral molecule are almost symmetric with respect to the diagonal ( $\xi_{mn} \approx \xi_{nm}$ ). This means that there is no preferable direction of motion for electron (or holes). The size of the mode along the ‘anti-diagonal’ ( $m - n$ ) direction reflects the delocalization of the relative motion of the electron-hole pair (exciton coherence size) whereas the variation along the diagonal reflects their center of mass motion (i.e. where the optical excitation resides within the molecule). We shall denote these the off-diagonal and diagonal sizes, respectively.

A more detailed view of the charge-density-wave i.e. the variation of the diagonal elements for modes  $\xi_{a'}$  and  $\xi_{b'}$  are given in panels F and G of Fig. 5 (This is a complementary information to Fig. 8 which only gives the absolute magnitudes of the density matrix elements and does not show their sign). Optical excitations of a neutral molecule are localized on the polyenic chain, with no significant change in mode structures as the chain-length is increased.  $\xi_{a'}$  is a *bulk mode* with an off-diagonal coherence size (i.e. size, where the amplitudes of coherences decrease to 10% of their maximum values) of about 12 double bonds. The dipole moment  $\mu_{a'} = Tr(\mu \xi_{a'})$  of this mode is uniformly distributed along the chain (see Fig. 9). We previously observed such bulk features in the band-edge transition of polyacetylene oligomers [17]. The second oscillator  $\xi_{b'}$  is very different: It has the same off-diagonal coherence size, but a non-uniform diagonal space distribution. Three contributions to the dipole moment are clearly identified  $\mu_{b'} = Tr(\mu \xi_{b'}) = \mu_I + \mu_{II} + \mu_{III}$ . The distribution of the dipole moment for these three regions is schemati-

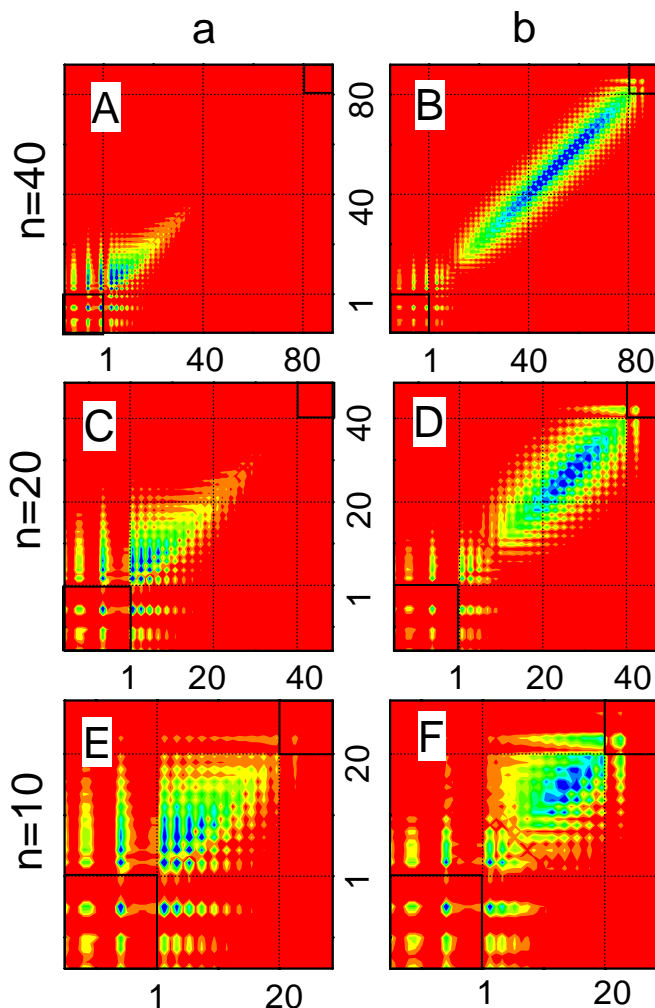


FIG. 10. Contour plots of density matrices for polar  $P(n)$  molecule. Top panels: coordinates of the first  $a$  (A) and second  $b$  (B) absorption peaks for chain length  $n = 40$  double bonds. Middle and bottom panels display the same quantities but for chain length  $n = 20$  and  $n = 10$  double bonds, respectively. The structures at the ends of molecules are shown by rectangles.

cally shown in Fig. 9. The strongest electronic coherences are created at the end regions of the molecule ( $I$  and  $III$ ) with diagonal size of about 17 double bonds. Weaker bridge coherences are created in the middle of the chain ( $II$ ). The total contribution from the ends is approximately zero, and only the region  $II$  contributes to the oscillator strength of this mode. This mode therefore makes only a weak contribution to the linear absorption. However, such *charge transfer* modes have the potential to dominate spectra of nonsymmetric structures.

The electronic modes  $\xi_a$  and  $\xi_b$  of the two oscillators contributing to the linear spectra of the polar molecules  $P(40)$ ,  $P(20)$ , and  $P(10)$  are displayed in Fig. 10. The diagonal elements of modes  $\xi_a$  and  $\xi_b$  in  $P(40)$  are shown in panels D and C of Fig. 5. Fig. 10A shows that the lowest peak (a) in  $P(40)$  represents a charge-transfer mode,

completely localized at the acceptor end with the same off-diagonal and diagonal sizes (12 and 17 double bonds respectively) as for the neutral molecule. The principal difference is the appearance of strong electronic coherences at the acceptor end. The coherences are more pronounced in the electron (ordinate) direction. This implies that the created electron-hole pair involves electron transfer from the acceptor to the chain. The hole resides primarily on the acceptor, whereas the electron can move also in region I of the bridge. This tends to reduce the chain-to-the acceptor electron transfer which takes place in the ground state. The dipole moment of the mode is large and localized (see Fig. 9). This mode therefore carries a strong oscillator strength in the optical response of small chains, and saturates (become constant) in larger molecules ( $n > 17$  double bonds). The second bulk mode (b) (Fig. 2B) differs only by the part controlled by acceptor from the bulk mode of neutral molecule (compared to Fig. 8A). The oscillator - strength of this mode for molecules with  $n > 12$  double bonds grows linearly. The absorption spectra of small chains are therefore controlled by the charge-transfer mode (a) whereas the bulk mode (b) becomes dominant with increasing molecular size. The different character of these modes is lost for chains shorter than effective coherence size of 12 double bonds such as P(10) displayed in Fig. 10(E,F). Quantum confinement [34] then dramatically affects the modes and we can no longer classify them as either end or bridge type. This is clearly evident by starting with large chains and gradually reducing the size.

#### IV. THE GROUND STATE OF LARGE MOLECULES: SOLITONS

Our study allows us to draw some general conclusions with regard to the ground state of large molecules. Panels A-C of Fig.11 display schematically the bond-length alternation pattern of several molecules with increasing acceptor strength. The ground state of an infinitely long molecule is represented by a bond-order wave which gives  $q_A = 0$ ,  $\delta l_n = \pm\delta\bar{l}$ . This means that the ground state is doubly degenerate with either  $\delta l_n = +\delta\bar{l}$  (double-single alternation) or  $\delta l_n = -\delta\bar{l}$  (single-double alternation). In finite molecules, the ground state degeneracy may be broken even if the molecules are very long. In neutral polyenes  $q_A = 0$  at the ends as well as in the bulk, which implies the formation of double bonds at the ends, giving  $\delta l_I > 0$  and  $\delta l_{III} > 0$ . Our calculations show that  $\delta l_I = \delta l_{III} \approx \delta l_{II}$ . The bond alternation in the bulk can assume two values,  $\delta l_{II} = \pm\delta\bar{l}$ . However if  $\delta l_{II} = -\delta\bar{l}$ , two solitons are needed to transform the boundary values  $\delta l_I = \delta l_{III} \approx \delta\bar{l}$  to the bulk values  $\delta l_{II} = -\delta\bar{l}$  (see Fig.11A) which means that the energy of the  $\delta l_{II} = -\delta\bar{l}$  configuration is higher than that of the  $\delta l_{II} = \delta\bar{l}$  configuration (Fig.11A) by the energy needed to form two solitons. The ground state is no longer degenerate and is represented by a homogeneous solution  $\delta l_{II} = \delta\bar{l}$ . This

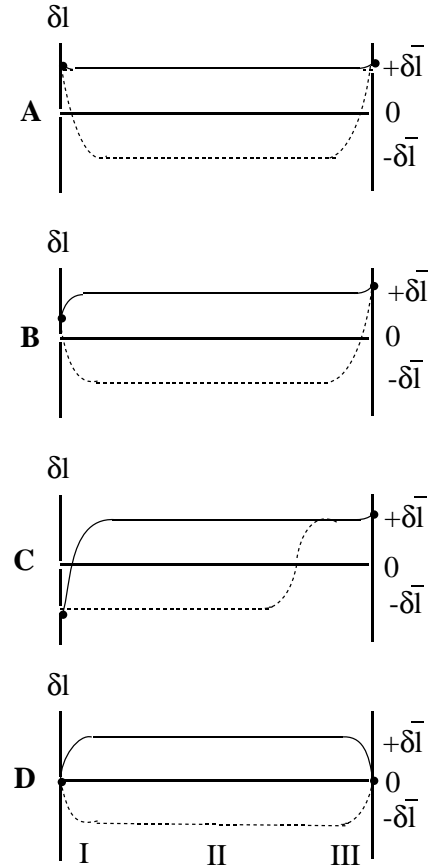


FIG. 11. Schematic variation of bond - length alternation pattern in the long acceptor substituted molecules with increasing acceptor strength (panels A to C). Two possible configurations corresponding to ground states with  $\delta l_{II} = \delta\bar{l}$  and  $\delta l_{II} = -\delta\bar{l}$  are shown by solid and dashed lines respectively. Panel A. No acceptor, the ground state in non-degenerate and has to  $\delta l_{II} = \delta\bar{l}$  (solid line), the state with  $\delta l_{II} = -\delta\bar{l}$  (dashed line) has a higher energy needed to form two solitons. Panel B Intermediate-strength acceptor: the ground state with  $\delta l_{II} = \delta\bar{l}$  is nondegenerate (solid line) and contains a soliton in the acceptor region. A state with  $\delta l_{II} = -\delta\bar{l}$  (dashed line) contains two solitons and has a higher energy. Panel C. Very strong acceptor; The molecule is separated into the acceptor with the charge  $-e$  and anion with the charge  $+e$  and (N-1) carbon atoms with the ground state representing the charged soliton. The ground state of an anion may become degenerate since a soliton can be formed anywhere (this is represented by the dashed line). However Coulomb interaction between the acceptor and the soliton leads to its localization near the acceptor (solid line). Panel D: Molecule substituted by a donor and an acceptor of intermediate strength. Two ground states with  $\delta l_{II} = \delta\bar{l}$  (solid line) and  $\delta l_{II} = -\delta\bar{l}$  (dashed line) have the same energy (cyanine like).

illustrates that the nondegeneracy of the ground state of linear conjugated molecules may be attributed to boundary effects.

By adding an acceptor to one end of a long molecule, we still have  $q_{III} = 0$ ,  $\delta l_{III} \approx \delta\bar{l}$ , however the charge

density at the acceptor end is  $q_I \neq 0$ . This leads to a decrease in the double chemical bond strength at that end, which implies that  $\delta l_I < \delta \bar{l}$ . If the acceptor is not very strong, a soliton is needed to transform  $\delta l = \delta l_I$  to its bulk value,  $\delta l = \delta l_{II} = \delta \bar{l}$ , and no soliton is needed at the other end (solid curve in Fig. 11B). This is confirmed by our calculations (see Fig. 5A). The soliton is located at the acceptor end of the molecule to minimize the length of the region where  $\delta l$  is different from its bulk value. The soliton size represents the length of the region where the boundary value of  $\delta l_I$  transforms to its bulk value. Charge screening occurs in the same region, as is clearly shown in Fig. 5B and C. A configuration with  $\delta l_{II} = -\delta \bar{l}$  (dashed lines in Fig. 11B) involves the formation of solitons on both ends and has a higher energy. The strong acceptor case is displayed in Fig. 11C. In this case we have  $\delta l_I = -\delta \bar{l}$  and the acceptor attracts an additional electron and the molecule is separated into two parts: the edge carbon atom (with charge  $-e$ ) and a polyacetylene anion which contains an odd  $(N - 1)$  number of carbon atoms and charge  $+e$ . The ground state of an anion (known as a charge soliton) [41,42] is needed to change the sign of the bond - length alternation  $\delta l = \pm \delta \bar{l}$  on the ends of the molecule. The charge  $+e$  is concentrated in the region where  $\delta l$  undergoes the change from  $-\delta \bar{l}$  to  $+\delta \bar{l}$ . The center of this region,  $x_0$ , and size of the region,  $\Delta x$ , are usually referred to as the soliton position and size respectively. The ground state is highly degenerate since the soliton can be found anywhere along the molecule (a typical situation is represented by the dashed line in Fig. 11C). This leads to the formation of a soliton band in the ground state. The ground state closely resembles the charged solitons observed in the ground state of anions of degenerate polymers molecules with odd numbers of carbon atoms [41]. However the Coulomb interaction between the charged acceptor and the soliton may lead to localization of the soliton in the vicinity of the edge (solid line in Fig. 11D). Decreasing the acceptor strength leads to a reduction of the absolute value,  $q$ , of charge accepted by the edge atom ( $q_A < e$ ) and to the appearance of bonding between the acceptor and the anion, which leads to  $-\delta \bar{l} < \delta l_I < \delta \bar{l}$ . This situation, which has been considered above, can be qualitatively represented as follows: a charged soliton is located at  $x_0 < \Delta x/2$  and is cut at  $x = 0$  (the acceptor position) since there are no carbon atoms at  $x < 0$ . If  $\delta l(x - x_0)$  is the soliton profile then  $\delta l_I = \delta l(x - x_0)$  and  $q_A < e$  is the charge in the soliton in the region  $-x_0 < x < \infty$ . Note that  $x_0$  can assume negative values as well. The weaker the acceptor, the smaller is  $x_0$ : decreasing  $x_0$  leads to the decrease of  $q_A$  and increase of  $\delta l_I$ . In the case of a very weak acceptor,  $x_0 \rightarrow -\infty$  (i.e.  $q_A \rightarrow 0$ ,  $\delta l_I \rightarrow \delta \bar{l}$ ). An intermediate case represented in Fig. 11D corresponds to  $x_0 = 0$ .

If we add an acceptor to one end (I) and a donor to the other end (III), the ground state degeneracy should occur at some intermediate donor and acceptor strength corresponding to  $\delta l_I \approx \delta l_{III} \approx 0$ . Two configurations corresponding to ground states with  $\delta l_{II} = \pm \delta \bar{l}$  are shown

in Fig. 11D. However in short molecules ( $L < \Delta x$ ) the ground state will then be non-alternating with  $\delta l = 0$ . This is known as the cyanine limit [43].

## V. DISCUSSION

The optical response of long acceptor-substituted molecules can be interpreted by dividing them into three effective regions: the acceptor (I) and the neutral (III) boundary transition regions at the molecular ends, connected by the bridge (middle) region (II). (In donor-acceptor substituted molecules, which were not considered here, region III will represent the donor end.) There is no charge transfer between these regions, which means that the optical properties are additive and can be interpreted in the same way as those of molecular aggregates [44]. Region II has the same properties as the neutral molecule; it has only odd order responses which scale linearly with size whereas regions I and III have a fixed size. The ground and the excited states are zwitteronic. These effective regions are responsible for even-order optical responses which naturally do not depend on the size of the underlying molecule. They contribute to odd-order response as well, but for long chains these responses are dominated by the region II contribution which is proportional to the size. For long chains the influence of the acceptor has a finite range which leads to the creation of several coherence sizes. The first coherence length,  $L_I$ , is related to the size on which the acceptor charge is screened; our calculations show that the bond-length alternation,  $\delta l$ , is different from its bulk value in the same region, hereafter referred to as the transition region. The acceptor may affect the excited states by either modifying an existing delocalized state in the transition region or creating new localized states at that region. Both mechanisms affect optical properties, and in particular they lead to a non-zero second-order polarizability  $\beta$ . We expect that the energy of a delocalized state should not be affected by the acceptor, whereas the energy of a localized state should strongly depend on the acceptor strength. This implies that localized and delocalized states may be readily distinguished by resonant three-wave mixing spectroscopies.

Optical properties of short molecules can be interpreted in terms of quantum confinement when the molecular size becomes comparable with the sizes  $L_I$  and  $L_{III}$  of the I and III - regions. These constitute additional coherence diagonal sizes, as opposed to the coherence off-diagonal size of the neutral molecule,  $L_{II}$ , represented by the width of its bulk mode (see Fig. 2F). In this case the electronic eigenstates of regions I, II, and III are mixed (see Fig. 8C and D) and for smaller sizes the separation into effective subunits is no longer possible since charge transfer takes place across the entire molecule (see Fig. 8A and B). The local excitation created by the acceptor drastically increases the polarizabilities of polyenic

molecules. The  $\pi$ -electronic system screens the acceptor influence: the acceptor strength controls the magnitude of the dipole moment whereas the electronic mobility determines the effective screening length.

The present approach should be particularly suitable for incorporating nuclear motions [45] by including additional nuclear oscillators. The time dependent density matrix will then allow us to follow the bond rearrangement in real time, coherent vibrations, solvent modes, and isomerization. These effects may be probed using femtosecond techniques [46,23,51,52]. Recent optical studies of dendrimers have raised interesting questions with regard to the localization of optical excitations [47]. The present approach should allow us to address this issue properly in a direct and unambiguous way.

### ACKNOWLEDGMENTS

We wish to thank Prof. W. E. Torruellas for most valuable discussions, and Prof. M. C. Zerner for providing us with the ZINDO program and for his help in using it. The support of the Air Force Office of Scientific Research, the National Science Foundation Center for Photoinduced Charge Transfer, and the National Science Foundation through Grants No. CHE-9526125 and No. PHY94-15583 is gratefully acknowledged. The calculations were conducted using the resources of the Cornell Theory Center, which receives major funding from the NSF and New York State.

### APPENDIX A: THE INTERMEDIATE NEGLECT OF DIFFERENTIAL OVERLAP / SPECTROSCOPY (INDO/S) HAMILTONIAN

We consider a general system of  $N$  electrons which can occupy  $K$  possible molecular states ( $N \leq K$ ) and interact with an external field. The eigenstates of the molecular electronic Hamiltonian

$$\hat{H}\Psi = E\Psi, \quad (\text{A1})$$

are approximated as a single Slater determinant  $\Psi = |\phi_1(1)\phi_2(2)\dots\phi_N(N)\rangle$ , where  $\{\phi_i\}$  are the molecular orbitals. Following Roothaan's procedure [28] they are expanded as a linear combination of known spatial atomic basis functions  $\{\chi_\alpha\}$

$$\phi_i = \sum_{\alpha}^K C_{i\alpha}\chi_{\alpha}. \quad (\text{A2})$$

The electronic Hamiltonian assumes the form [28]

$$\begin{aligned} \hat{H} = & \sum_{mn\sigma} t_{mn} c_{m\sigma}^+ c_{n\sigma} + \sum_{\substack{m n k l \\ \sigma \sigma'}} \langle nm|kl\rangle c_{m\sigma}^+ c_{n\sigma'}^+ c_{k\sigma'} c_{l\sigma} \\ & - \mathcal{E}(t) \sum_{mn\sigma} \mu_{mn} c_{m\sigma}^+ c_{n\sigma}, \end{aligned} \quad (\text{A3})$$

where subscripts  $i, j, k, l$  run over atomic basis functions and  $\sigma, \sigma'$  label spin components.  $c_n^+$  ( $c_n$ ) are the creation (annihilation) operators which satisfy the Fermi anticommutation relations in the orthogonal basis set

$$c_{m\sigma} c_{n\sigma'}^+ + c_{n\sigma'}^+ c_{m\sigma} = \delta_{mn} \delta_{\sigma\sigma'}, \quad (\text{A4})$$

and all other anticommutators of  $c^+$  and  $c$  vanish. Hereafter we will focus on the closed-shell case and exclude spin variables [28]. Generalization to the unrestricted open-shell case is straightforward.

The first term in Eq. (A3) is the core-hamiltonian describing the kinetic energy and nuclear attraction of an electron

$$\begin{aligned} t_{nm} = & \langle n | -\frac{1}{2}\nabla_1^2 - \sum_A \frac{Z_A}{|\mathbf{r}_1 - \mathbf{R}_A|} | m \rangle \\ \equiv & \int d\mathbf{r}_1 \chi_n^*(1) \left( \nabla_1^2 - \sum_A \frac{Z_A}{|\mathbf{r}_1 - \mathbf{R}_A|} \right) \chi_m(1), \end{aligned} \quad (\text{A5})$$

where  $\mathbf{R}_A$  is the nuclear coordinate of atom  $A$ . The second term represents electron-electron Coulomb interactions where

$$\langle nm|kl\rangle = \int d\mathbf{r}_1 d\mathbf{r}_2 \chi_n^*(1) \chi_m^*(2) \frac{1}{r_{12}} \chi_k(1) \chi_l(2) \quad (\text{A6})$$

are the two-electron integrals. The interaction between the electrons and the external electric field  $\mathcal{E}(\mathbf{t})$  polarized along the chosen  $z$ -axis is given by the last term in Eq. (A3),  $\mu$  being the dipole operator

$$\mu_{nm} = \langle n | \mu_z | m \rangle \equiv \int d\mathbf{r}_1 \chi_n^*(1) z_1 \chi_m(1). \quad (\text{A7})$$

The SCF procedure used to solve the Schrödinger equation (A1) for the Hartree-Fock ground state [28] is based on the iterative solution of the matrix equation

$$FC = C\epsilon. \quad (\text{A8})$$

This equation may be recast in the form

$$[F(\bar{\rho}), \bar{\rho}] = 0, \quad (\text{A9})$$

where the ground-state density matrix is related to the molecular orbital expansion coefficients (Eq. (A2)) as

$$\bar{\rho}_{nm} = 2 \sum_a^{N/2} C_{na} C_{ma}^*. \quad (\text{A10})$$

$F(\bar{\rho})$  is the Fock matrix

$$F(\bar{\rho}) = t + V(\bar{\rho}), \quad (\text{A11})$$

and the matrix representation of the Coulomb electronic operator  $V$  in the atomic basis set  $\{\chi_\alpha\}$  is

$$V(\bar{\rho})_{mn} = \sum_{k,l}^K \bar{\rho}_{kl} [\langle mk|nl\rangle - \frac{1}{2}\langle mn|kl\rangle]. \quad (\text{A12})$$

The INDO approximation [49] limits the basis set to valence orbitals of Slater type. These atomic orbitals are assumed to be orthogonal

$$\langle n|m \rangle = \int d\mathbf{r}_1 \chi_n^*(1) \chi_m(1) = \delta_{nm}, \quad (\text{A13})$$

and the exchange terms in the two-electron interaction are permitted only among orbitals located on the same atom

$$\langle \chi_n^A \chi_k^B | \chi_m^A \chi_l^B \rangle = \begin{cases} \langle \chi_n^A \chi_k^A | \chi_m^A \chi_l^A \rangle & A = B \\ \langle \chi_n^A \chi_k^B | \chi_m^A \chi_l^B \rangle \delta_{nm} \delta_{kl} & A \neq B \end{cases} \quad (\text{A14})$$

where  $\chi_n^A$  belongs to atom A and  $\chi_n^B$  to atom B. The four-dimensional matrix  $\langle \chi_n \chi_k | \chi_m \chi_l \rangle$  thus becomes block-diagonal in two dimensions. The parameters of the INDO/S hamiltonian are given in [49,50,53].

## APPENDIX B: THE SINGLE-ELECTRON DENSITY MATRIX AND THE TDHF EQUATIONS

The TDHF approach provides a convenient approximation scheme for calculating the optical response of large molecules. The reduced single-electron density matrix Eq. (1.1) representing the molecule driven by an external field is given by  $\rho(t) = \bar{\rho} + \delta\rho(t)$  where the ground-state density matrix  $\bar{\rho}$  is the key input to this calculations. The diagonal element of  $\rho_{nm}$  ( $n = m$ ) represents the charge at the  $m$ 'th atomic orbital, and

$$q_A = \sum_{n \in A} \bar{\rho}_{nn} - Z_A \quad (\text{B1})$$

is the net charge on the atom A. The off-diagonal elements ( $n \neq m$ ) represent the electronic coherences between atomic orbitals. In particular,  $\bar{\rho}_{n_A m_B}$  describe the chemical bonding strength (bond-order) between atoms A and B. The matrix elements of  $\delta\rho_{nm}(t)$  represent the changes in these quantities induced by the electric field.

We start with the Heisenberg equation of motion for  $c_n^+ c_m$ . This equation is not closed since higher order products will show up in the right hand side. Writing equations of motion for these higher products will yield increasingly higher products. This is the famous hierarchy of many-body dynamics that is common to classical and quantum mechanics. To overcome this difficulty we need a truncation procedure. The simplest assumes that the many-body wavefunction is given by a single Slater determinant at all times. This yields the time dependent Hartree-Fock factorization [48,15,18]

$$\begin{aligned} \langle c_n^+ c_m^+ c_{n'} c_{m'} \rangle(t) &= \langle c_n^+ c_{n'} \rangle \langle c_m^+ c_{m'} \rangle(t) \\ &+ \langle c_n^+ c_{m'} \rangle \langle c_m^+ c_{n'} \rangle(t) \end{aligned} \quad (\text{B2})$$

To derive equations of motion we first decompose  $\delta\rho(t)$  into two components

$$\delta\rho(t) = \xi(t) + T(\xi(t)), \quad (\text{B3})$$

where  $\xi$  represents the particle-hole (interband) and  $T(\xi)$  represents the particle-particle and the hole-hole (intra-band) parts. The dimensionality of density matrix  $\rho$  defined by the basis set size is  $K \times K$ . We assume  $N$  occupied and  $K - N$  unoccupied orbitals. The dimensionality of interband and intraband parts are  $2N(K - N)$  and  $N^2 + (K - N)^2$  respectively. The projection property of the reduced single-electron density matrix  $\rho(t)^2 = \rho(t)$  makes it possible to express  $T(\xi)$  in terms of  $\xi$

$$T(\xi) = \left( \bar{\rho} - \frac{I}{2} \right) \left( I - \sqrt{I - 4\xi^2} \right), \quad (\text{B4})$$

where  $I$  is the unit  $K \times K$  matrix.

Applying the TDHF ansatz Eq. (B2) we obtain the following closed equations of motion for  $\xi$ .

$$i \frac{\partial \xi}{\partial t} - L\xi = R(\xi)_{p-h} - \mathcal{E}(t) \cdot [\mu, \bar{\rho}], \quad (\text{B5})$$

where  $L$  is a linear operator in Liouville space (i.e. superoperator) [15,18,17] given by

$$L\xi = [F(\bar{\rho}), \xi] + [V(\xi), \bar{\rho}], \quad (\text{B6})$$

and

$$\begin{aligned} R(\xi) &= [F(\xi), \xi + T(\xi)] + [F(T(\xi)), \bar{\rho} + \xi] \\ &- \mathcal{E} \cdot [\mu, \xi + T(\xi)] \end{aligned} \quad (\text{B7})$$

is the nonlinear part of the equation projected onto the particle-hole subspace (Eq. (C2)). The Fock operator  $F$  and the Coulomb operator  $V$  are defined by Eqs (A11) and (A12).

The time-dependent polarization which determines all optical properties is finally given by

$$P(t) = Tr(\mu\xi(t)) + Tr(\mu T(\xi(t))). \quad (\text{B8})$$

Eqs. (B5) and (B4) constitute the basic TDHF equations [18]. They may be solved by expanding the density matrix in powers of the external field

$$\begin{aligned} \xi &= \xi^{(1)} + \xi^{(2)} + \dots, \\ T(\xi) &= T^{(2)}(\xi) + T^{(3)}(\xi) + \dots \end{aligned} \quad (\text{B9})$$

The original nonlinear equation (B5) is then transformed into a hierarchy of linear inhomogeneous equations. To  $j$ -th order we have

$$i \frac{\partial \xi^{(j)}(t)}{\partial t} - L\xi^{(j)}(t) = \eta^{(j)}(t), \quad (\text{B10})$$

where  $\eta^{(j)}(t)$  is given in terms of  $\bar{\rho}$  and lower order  $\xi^{(k)}$   $k < j$ ,  $\eta^{(1)}(t) = -\mathcal{E}(t)[\mu, \bar{\rho}]$ , etc.

The linear and non-linear optical response is calculated by solving Eq. (B10) either in the frequency domain or in the time domain. In the frequency domain, the procedure

involves diagonalizing the linearized Liouville operator  $L$  which requires a large memory ( $\sim N^4$  where  $N$  is the total number of orbitals in the system). Time-domain calculations do not require a large memory ( $\sim N^2$ ) and may be applied for larger systems. However evaluating commutators in Eqs. (B6) and (B7) is time consuming. These difficulties limit the application of the TDHF to basis set size of about 100 functions.

### APPENDIX C: THE ELECTRONIC NORMAL MODES

In this Appendix we review a few properties of the tetradic linear  $M_0 = N(K - N)$  dimensional space defined by the Liouville operator  $L$  and constrained by the projection property of the reduced single-electron density matrix  $\rho(t)$  [18,17,15].

The scalar product of any two interband  $K \times K$  matrices  $A$  and  $B$  which are the elements of this space is given by [18,17]

$$\langle A|B \rangle \equiv Tr(\bar{\rho}[A, B]). \quad (C1)$$

Note that  $\langle A|B \rangle = -\langle B|A \rangle$ . This scalar product thus behaves more as a classical Poisson bracket rather than a quantum mechanical scalar product. The projection property of  $\bar{\rho}$  allows us to project any matrix  $A$  into the particle-hole subspace

$$A_{p-h} = [[A, \bar{\rho}], \bar{\rho}]. \quad (C2)$$

The eigenmodes  $\xi_\nu$  and eigenfrequencies  $\Omega_\nu$  of  $L$  satisfy the equation.

$$L\xi_\nu = \Omega_\nu\xi_\nu \quad L\xi_\nu^+ = -\Omega_\nu\xi_\nu^+, \quad \nu = 1, \dots, M_0. \quad (C3)$$

The eigenmodes come in conjugate pairs: Each vector  $\xi_\nu$  with frequency  $\Omega_\nu$  has a counterpart  $\xi_{-\nu} = \xi_\nu^+$  with frequency  $-\Omega_\nu$ . Since  $L$  is real, the electronic modes can be taken to be real as well. A classical mode picture of the optical response is obtained by constructing the electronic oscillators defined by the coordinate-momentum variables

$$Q_\nu = \frac{\xi_\nu + \xi_\nu^+}{\sqrt{2}}, \quad P_\nu = -i\frac{\xi_\nu - \xi_\nu^+}{\sqrt{2}}. \quad (C4)$$

$P$  and  $Q$  satisfy the relation

$$LQ_\nu = \Omega_\nu iP_\nu, \quad LiP_\nu = \Omega_\nu Q_\nu, \quad \nu = 1, \dots, M_0. \quad (C5)$$

We shall adopt the following normalization of the electronic modes [18]:

$$\langle \xi_\alpha^+ | \xi_\beta \rangle = \delta_{\alpha\beta}, \quad \langle \xi_\alpha^+ | \xi_\alpha^+ \rangle = 0; \quad (C6)$$

$$\langle P_\alpha | Q_\beta \rangle = i\delta_{\alpha\beta}, \quad \langle P_\alpha | P_\beta \rangle = \langle Q_\alpha | Q_\beta \rangle = 0. \quad (C7)$$

The electronic oscillator is a pair of conjugated electronic modes ( $K \times K$  matrices  $\xi_\nu$  and  $\xi_\nu^+$  or  $P_\nu$  and  $Q_\nu$ ) with the frequency  $\Omega_\nu$ . Any interband  $K \times K$  matrix  $A$  can be expanded in the basis set of electronic oscillators as

$$\begin{aligned} A &= \sum_{\nu=1}^{M_0} \langle \xi_\nu^+ | A \rangle \xi_\nu - \langle \xi_\nu | A \rangle \xi_\nu^+ \\ &= \sum_{\nu=1}^{M_0} \langle Q_\nu | A \rangle iP_\nu - \langle iP_\nu | A \rangle Q_\nu. \end{aligned} \quad (C8)$$

### APPENDIX D: THE DENSITY-MATRIX-SPECTRAL-MOMENT ALGORITHM (DSMA)

The Density-Matrix-Spectral-Moments Algorithm (DSMA) [17] is an approximate scheme for solving the TDHF equations which allows us to calculate  $\xi^{(j)}$  from the source ( $\eta^{(j)}$ ) by solving Eq. (B10) without a direct diagonalization of  $L$ . This is accomplished by computing the set of electronic oscillators which dominate the expansion of  $\eta^{(j)}$ . We can take  $\eta^{(j)}(t)$  to be real and express it in terms of our momentum variables as [17]

$$\begin{aligned} \eta^{(j)} &= \sum_{\nu=1}^{M_0} \langle \xi_\nu^+ | \eta^{(j)} \rangle \xi_\nu - \langle \xi_\nu | \eta^{(j)} \rangle \xi_\nu^+ \\ &= \sum_{\nu=1}^{M_0} \langle Q_\nu | \eta^{(j)} \rangle iP_\nu = \sum_{\nu=1}^{M_0} \mu_\nu^{(j)} iP_\nu, \end{aligned} \quad (D1)$$

where  $\eta^{(j)}$  can be viewed either in the frequency or in the time domain, and  $\mu_\nu^{(j)} = \sqrt{2}\langle \xi_\nu | \eta^{(j)} \rangle = \langle Q_\nu | \eta^{(j)} \rangle$  are the real frequency (or time) dependent expansion coefficients. These electronic oscillators provide a convenient procedure for solving Eq. (B10) [18]. The formal solutions of Eq. (B10) in the time and frequency domain are

$$\begin{aligned} \xi^{(j)}(t) &= \int_0^t d\tau e^{-iL(t-\tau)} \eta^{(j)}(\tau), \\ \xi^{(j)}(\omega) &= \frac{1}{\omega - L} \eta^{(j)}(\omega). \end{aligned} \quad (D2)$$

Substituting to these equations the expansion (D1) for  $\eta^{(j)}$  and utilizing the eigenvector properties of the modes

$$\begin{aligned} e^{-iLt}\xi_\nu &= e^{-i\Omega_\nu t}\xi_\nu, \quad e^{-iLt}\xi_\nu^+ = e^{i\Omega_\nu t}\xi_\nu^+; \\ \frac{1}{\omega - L}\xi_\nu &= \frac{1}{\omega - \Omega_\nu}\xi_\nu, \quad \frac{1}{\omega - L}\xi_\nu^+ = \frac{1}{\omega + \Omega_\nu}\xi_\nu^+ \end{aligned} \quad (D3)$$

we obtain the solution of Eq. (B10) in terms of eigenmodes  $\xi_\nu$  and  $\xi_\nu^+$  (or  $P_\nu$  and  $Q_\nu$ ). For example, the  $j$ -th order interband component of the reduced single-electron density matrix in frequency domain is given by

$$\xi^{(j)}(\omega) = \sum_{\nu=1}^{M_0} \mu_\nu^{(j)}(\omega) \left[ \frac{\Omega_\nu}{\Omega_\nu^2 - \omega^2} Q_\nu - \frac{i\omega}{\Omega_\nu^2 - \omega^2} P_\nu \right]. \quad (D4)$$

Since only few electronic oscillators contribute significantly to the source in the expansion (D1), the summation can be truncated at some effective number of oscillators  $M \ll M_0$  without sacrificing accuracy.

The family of the density-matrix spectral moments is defined as  $S_n \equiv L^n \eta$ . These moments are used to construct the main DSMA equations [17]

$$S_n^{(j)} = \sum_{\nu=1}^M \Omega_\nu^n \mu_\nu^{(j)} i P_\nu, \quad n = 0, 2, 4, \dots, 2M - 2, \quad (\text{D5})$$

$$S_n^{(j)} = \sum_{\nu=1}^M \Omega_\nu^n \mu_\nu^{(j)} Q_\nu, \quad n = 1, 3, 5, \dots, 2M - 1, \quad (\text{D6})$$

where  $S_0^{(j)} = \eta^{(j)}$  and  $S_n^{(j)} = L^n S_0^{(j)}$ ,  $n = 1, 2, \dots$

The scalar products  $\mathcal{K}_n^{(j)} \equiv \langle S_n^{(j)} | S_{n+1}^{(j)} \rangle$ ,  $n = 1, 2, \dots, 2M$  provide a set of equations for the frequencies  $\Omega_\nu$  and oscillator strength  $f_\nu^{(j)} = (\mu_\nu^{(j)})^2 \Omega_\nu$ :

$$\sum_{\nu=1}^M f_\nu^{(j)} \Omega_\nu^{2n} = \mathcal{K}_n^{(j)} \quad n = 0, 1, 2, \dots, 2M - 1. \quad (\text{D7})$$

The set of DSMA equations [(D5)-(D7)] is now complete. We start our calculations by computing the moments  $S_n^{(j)}$  and  $\mathcal{K}_n^{(j)}$  acting Liouville operator  $L$  (B6) on the source  $\eta^{(j)}$  and using definition of the scalar product (C1). We then solve Eqs. (D7) for the frequencies  $\Omega_\nu$  and oscillator strengths  $f_\nu^{(j)}$ . These equations are nonlinear but have a simple analytical solution (Appendix B in [17]). Once we have  $\Omega_\nu$  and  $\mu_\nu^{(j)}$ , we solve (D5) and (D6) for the modes  $P_\nu$  and  $Q_\nu$ . The most time consuming part of the DSMA is the calculation of commutators. Typically only a small number of modes is required and the DSMA greatly reduces the numerical effort involving in solving the complete TDHF equations.

Because of truncation at  $M$  oscillators, the resulting electronic modes do not coincide with the TDHF modes. Eqs. (C5) hold approximately, but the normalization relations (C7) are satisfied exactly. These effective electronic oscillators give the best approximation for the spectrum with a given number of features ( $M$ ). A notable advantage of the DSMA is that we immediately obtain a global overview of the entire spectrum. However we cannot increase the number of effective oscillators  $M$  at will to improve the accuracy. High moments scale exponentially ( $\mathcal{K}_n \sim \Omega^{2n}$ ) and are dominated by high frequencies. Therefore increasing the number of oscillators does not refine the low and middle frequency range. In practice  $M$  is limited to  $\leq 10 - 14$ . Previous applications of the DSMA using the PPP hamiltonian which only describes the  $\pi$ -electron system allowed to calculate accurately spectra of polyens dominating by a few lines. The INDO/S hamiltonian includes also the valence electrons, therefore the source is not limited to  $\pi - \pi^*$  molecular excitations but also depends on a manifold of high-frequency atomic transitions. For molecules

with a complicated electronic structure the DSMA does not reproduce delicate spectral features such as excitations with a small oscillator strength. To improve the accuracy we have to apply the DSMA iteratively.

That the DSMA automatically generates orthonormal effective oscillators (Eqs. (C7)) which satisfy the eigenvalue equation (C5) in an optimal way. Therefore, each of the effective DSMA modes is a superposition of the exact TDHF modes with close frequencies. Thus the entire spectrum is divided into several regions. Each effective oscillator is responsible for part of spectrum and it is dominated by fewer exact oscillators than the initial source. This property allows to use any effective mode  $P_\nu$  as a new fictitious source term  $\eta = i P_\nu$  in the DSMA. The resulting oscillators are much closer to the exact ones. This procedure (i.e. using one of the new oscillators as a new fictitious source for the next DSMA level) can be repeated several times until some convergence criteria are satisfied. In practice this fictitious source is dominated by a single oscillator ( $P_1, Q_1$ ) which converges to the exact one. To recover the next mode, the same iterative procedure can be applied with one principal difference: all input sources must be made orthogonal to the lower modes. Thus by using

$$\eta_\perp = \eta - \sum_k^{\text{recovered}} \langle Q_k | \eta \rangle P_k, \quad (\text{D8})$$

we exclude all the recovered modes from the source in the following calculations. We can continue this iterative process utilizing this orthogonalization procedure to refine several electronic modes. This yields an expansion of the original source and allows us to focus on desirable fine features of the spectrum at high resolution.

In principle, the frequency(time)-dependent polarizabilities can be calculated by applying the DSMA to the frequency(time)-dependent source [Eq. (B5)]. This is difficult because hundreds DSMA runs are needed to scan accurately all frequency(time) region. In practice we calculate the off-resonant response first. The expressions for the different orders of static sources  $\eta^{(j)} = \eta^{(j)}(\omega = 0)$  and intraband components of density matrices  $T^{(j)} = T^{(j)}(\omega = 0)$  are given by Eqs. (25) and (26) in [17] or they may be derived by expanding Eqs. (B7) and (B4) in powers of  $\xi$ . We run the iterative DSMA for each order of the optical response. Calculations give us the sets of electronic oscillators ( $\Omega_\nu, P_\nu, Q_\nu$ ) which dominate  $j$ th order of responses ( $j = 1, 2, \dots$ ). The statically induced density matrix is given by

$$\xi^{(j)} = \sum_{\nu=1}^{M_0} \frac{\text{Tr}(\bar{\rho}[\eta_\nu^{(j)}, Q_\nu])}{\Omega_\nu} Q_\nu \quad (\text{D9})$$

and

$$\delta\rho^{(j)} = \xi^{(j)} + T(\xi^{(j-1)}, \xi^{(j-2)}, \dots). \quad (\text{D10})$$

The optical polarizabilities are readily obtained using Eq. (B8)

$$\chi^{(j)} = -\frac{1}{\mathcal{E}_o^k} \text{Tr}(\mu \delta \rho^{(j)}(\omega = 0)), \quad (\text{D11})$$

where  $\chi^{(1)} = \alpha(0)$ ,  $\chi^{(2)} = \beta(0)$ ,  $\chi^{(3)} = \gamma(0)$ , etc. The resulting electronic oscillators need to be used to construct frequency(time)-dependent optical response. Frequency-dependent response functions with up to the third order response are expressed through the electronic modes in [18] [Eqs. (5.6) and (E3)]. For example, oscillators dominating the first, second, and third orders off-resonant responses contributes to the three, two, and one-photon resonances in the resonant third order polarizability  $\gamma(-\omega; \omega_1, \omega_2, \omega_3)$ .

In summary, the DSMA calculates the optical response by solving the TDHF equations for motion of the single-electron density matrix. The algorithm consists of several levels of increasing complexity. First we recover the entire optical response with low resolution at extremely low computational cost. All strong transitions are fully recovered but the fine structure of spectrum is missing. The iterative DSMA provides more detailed information. We implemented the simplest version of this procedure to calculate the optical response of organic molecules. The band edge transition oscillator was calculated first. The remaining electronic oscillators were recovered sequentially with increasing frequency and were used to compute optical polarizabilities.<sup>3</sup> This approach allows us to recover accurately the experimentally relevant low-frequency spectral region (up to  $\sim 8$  eV).

- 
- [1] *Nonlinear Optical Properties of Organic Molecules and Crystals*, Vol. 1, 2, J. Zyss and D. S. Chemla, Eds. (Academic Press, Florida, 1987).
- [2] S. Speiser, *Chem. Rev.*, **97**, 1953 (1996).
- [3] V. Balzani and F. Scandola, *Supramolecular Photochemistry*, Ellis Harwood, NY (1991).
- [4] M. Blanchard - Desce, J.-M. Lehn, M. Barzoukas, C. Runser, A. Fort, G. Puccetti, I. Ledoux, and J. Zyss, *Nonlinear Optics*, **10**, 23 (1995).
- [5] M. Blanchard - Desce, R. Woltmann, S. Lebus, J.-M. Lehn, P. Kramer *Chem. Phys. Lett.*, **243**, 526 (1995).

---

<sup>3</sup>A more general (and complex) procedure is to focus on a limited frequency region, and pick up physically important modes by analyzing all the effective oscillators obtained at each iteration. The remaining modes are included in the dominant modes and only a few modes are necessary. In such a case we investigate the detailed structure of the chosen spectral region, but the algorithms for sorting out the effective electronic oscillators need to be developed for each particular case.

- [6] J. B. Birks, *Photophysics of Aromatic Molecules*, Wiley, New York (1970).
- [7] J. Michl and V. Bonacic-Koutecky, *Electronic Aspects of Organic Photochemistry*, Wiley, New York (1990); M. Klessinger and J. Michl, *Excited States and Photochemistry of Organic Molecules*, VCH, New York (1995).
- [8] G. U. Bublitz, R. Ortiz, S. R. Marder, S. G. Boxer, *JACS* **119**, 3365 (1997).
- [9] D. R. Kanis, M. A. Ratner, and T. J. Marks, *Chem. Rev.*, **94**, 195 (1994).
- [10] J. L. Brédas, C. Adant, P. Tackyx, A. Persoons, and B. M. Pierce, *Chem. Rev.* **94**, 243 (1994).
- [11] S. R. Marder, W. E. Torruellas, M. Blanchard - Desce, V. Ricci, G. I. Stegeman, S. Gilmour, J. L. Brédas, J. Li, G. U. Bublitz, S. G. Boxer, *Science* **276**, 1233 (1997).
- [12] M. Blanchard - Desce, C. Runser, A. Fort, M. Barzoukas, J.-M. Lehn, V. Bloy, V. Alain, *Chem. Phys.*, **199**, 253 (1995); M. Blanchard - Desce, J.-M. Lehn, M. Barzoukas, I. Ledoux, and J. Zyss, *Chem. Phys.*, **181**, 281 (1994).
- [13] M. C. Zerner, K. K. Stavrev, T. J. Meyer *JACS*, **117**, 8684 (1995).
- [14] A. Broo and M. C. Zerner, *Chem. Phys.*, **196**, 407 (1995); *ibid* **196**, 423 (1995).
- [15] A. Takahashi, S. Mukamel, *J. Chem. Phys.*, **100**, 2366 (1994); S. Mukamel, A. Takahashi, H. X. Wang, G. Chen, *Science*, **266**, 251 (1994).
- [16] S. Mukamel, S. Tretiak, T. Wagersreiter, and V. Chernyak, *Science*, **277**, 781 (1997).
- [17] S. Tretiak, V. Chernyak and S. Mukamel, *Chem. Phys. Lett.* **259**, 55 (1996); S. Tretiak, V. Chernyak and S. Mukamel, *J. Chem. Phys.*, **105**, 8914 (1996).
- [18] V. Chernyak, S. Mukamel, *J. Chem. Phys.* **104**, 444 (1996).
- [19] O. Straub, *Key to Carotenoids*, Basel; Boston: Birkhauser, 1987.
- [20] G. Britton, S. Liaaen-Jensen, and H. Pfander, (ed.) *Carotenoids*, Basel; Boston: Birkhauser 1995.
- [21] Y. Koyama and Y. Mukai *Biomolecular Spectroscopy, Part B* Edited by R.J.H. Clark and R.E. Hester, John Wiley & Sons Ltd, 1993.
- [22] A. Young and G. Britton, George (ed.), *Carotenoids in Photosynthesis*, Chapman and Hall, London, 1993.
- [23] R.A. Mathies, C.H. Brito Cruz, W.T. Pollard, and C. V. Shank, *Science*, **240**, 777 (1988).
- [24] G. Herzberg, *Electronic Spectra of Polyatomic Molecules* (Van Nostrand, Toronto, 1966).
- [25] J. F. Ward, *Rev. Mod. Phys.*, **37**, 1, (1965); B. J. Orr, J. F. Ward, *Mol. Phys.*, **20**, 513, (1971).
- [26] R. McWeeny and B.T. Sutcliffe, *Methods of Molecular Quantum Mechanics* (Academic Press, New York, 1976); E. R. Davidson, *Reduced Density Matrices in Quantum Chemistry* (Academic Press: New York, 1976); A. Szabo, N. A. Ostlund, *Modern Quantum Chemistry* (McGraw-Hill: New York, 1989).
- [27] H. White, *Phys. Rev. B*, (1994).
- [28] A. Szabo and N. S. Ostlund, *Modern Quantum Chemistry: Introduction to Advanced Electronic Structure Theory* (McGraw-Hill, New York, 1989).
- [29] R. S. Milliken, *J. Chem. Phys.*, **23**, 1833, 1841, 2338, 2343,

- (1955).
- [30] A. E. Reed, L. A. Curtiss, and F. Weinhold, *Chem. Rev.*, **88**, 899, (1988); A. E. Reed, R. B. Weinstock, and F. Weinhold, *J. Chem. Phys.*, **83**, 735, (1985).
- [31] P. O. Lowdin, *Phys. Rev.* **97**, 1474, (1955); *Adv. in Phys.* **5**, 1, (1956).
- [32] H. Haug and S. W. Koch, *Quantum Theory of the Optical and Electronic Properties of Semiconductors*, World Scientific, Singapore, 1994, 3rd ed.
- [33] W. L. Wilson, P. S. Szajowski, and L. E. Brus, *Science* **262**, 1242 (1993); L. E. Brus, Feature Article, *J. Chem. Phys.* **98**, 3575 (1994).
- [34] A. P. Alivisatos, *MRS bulletin*, **20**, 23 (1995); *Science* **271**, 993 (1996).
- [35] M. Nirmal, D. J. Norris, M. Kuno, M. G. Bawendi, Al. L. Efros, and M. Rosen, *Phys. Rev. Lett.*, **75**, 3728 (1995).
- [36] Vincent Ricci, *Large Enhancement of Third Order Susceptibility*, MS Thesis, Dept. of Electrical Engineering, University of Central Florida (1995).
- [37] H. Fukutome, *J. Mol. Struct. (Theochem)* **188**, 337 (1989), and references therein.
- [38] S. Tretiak, V. Chernyak, and S. Mukamel, *Phys. Rev. Lett.* **77**, 4656 (1996).
- [39] M. Yan, L.J. Rothberg, F. Papadimitrakopoulos, M.E. Galvin, and T.M. Miller, *Phys. Rev. Lett.* **72**, 1104, (1994); M. Yan, L.J. Rothberg, F. Papadimitrakopoulos, M.E. Galvin, and T.C. Miller, *Phys. Rev. Lett.* **73**, 744 (1994); M. Yan, L.J. Rothberg, E.W. Kwock, and T.M. Miller, *Phys. Rev. Lett.* **75**, 1992, (1995).
- [40] S. Mukamel and H. X. Wang, *Phys.Rev.Lett.*, **69**, 65 (1992).
- [41] A. J. Heeger, S. Kivelson, J. R. Schrieffer, and W. -P. Su, *Rev. Mod. Phys.*, **60**, 781 (1988).
- [42] A.Takahashi and S.Mukamel, *J. Chem. Phys.*, **103**, 7144-7155 (1995)
- [43] F. Meyers, S. R. Marder, B. M. Pierce, and J. L. Brédas, *JACS*, **116**, 10703 (1994); S. R. Marder, J. W. Perry, B. G. Tiemann, C. B. Gorman, S. Gilmour, S. L. Biddle, G. Bourhill, *JACS*, **115**, 2524 (1993).
- [44] S.Mukamel, *Principles of Nonlinear Optical Spectroscopy* (Oxford, New York, 1995).
- [45] G. Zerbi, V. Veronelli, S. Martina, A. D. Schlöter, and G. Wegner, *J. Chem. Phys.*, **100**, 978 (1994); G. Zerbi, E. Galbiati, M. C. Gallazzi, C. Castiglioni, M. Del Zoppo, R. Schenk, and K. Mölen, *J. Chem. Phys.*, **105**, 2509 (1996).
- [46] T. A. Pham, A. Daunois, J. -C. Merle, J. Le Moigne, and Y. -V. Bigot, *Phys. Rev. Lett.*, **74**, 904 (1995).
- [47] R. Kopelman, M. Shortreed, Z.-Y. Shi, W. Tan, Z. Xu, J. S. Moore, A. Bar-Haim, and J. Klafter, *Phys. Rev. Lett.*, **78**, 1239 (1997); A. Bar-Haim, J. Klafter, and R. Kopelman, *JACS* (submitted).
- [48] M. Hartmann, V. Chernyak, and S. Mukamel, *Phys. Rev. B*, **52**, 2528 (1995).
- [49] J. A. Pople and G. A. Segal *J. Chem. Phys.*, **43**, S136 (1965); J. A. Pople D. L. Beveridge, and P. Dobosh, *J. Chem. Phys.*, **47**, 2026 (1967).
- [50] J. Ridley and M. C. Zerner, *Theor. Chim. Acta*, **32**, 111 (1973).
- [51] J. B. van Beek, F. Kajzar, and A. C. Albrecht, *J. Chem. Phys.*, **95**, 6400 (1991); J. B. van Beek and A. C. Albrecht, *Chem. Phys. Lett.*, **187**, 269 (1991).
- [52] Z. G. Soos and D. Mukhopanhyay, *J. Chem. Phys.*, **101**, 5515 (1994).
- [53] M. C. Zerner, G. H. Loew, R. F. Kirchner, and U. T. Mueller - Westerhoff, *J. Am. Chem. Soc.*, **102**, 589 (1980).